

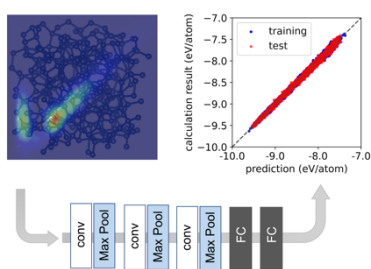
Persistent homology-based descriptor for machine-learning potential

Emi Minamitani^{1,2,3}, Ippei Obayashi^{3,4}

1. Institute for Molecular Science, Okazaki 444-8585, Japan
2. The Graduate University for Advanced Studies, Okazaki 444-8585, Japan
3. JST, PRESTO, Kawaguchi, Saitama 332-0012, Japan
4. Cyber-Physical Engineering Informatics Research Core (Cypher), Okayama University, Okayama 700-8530, Japan

Abstract

Constructing efficient descriptors that represent atomic configurations is crucial for developing a superior machine-learning potential. Widely used conventional descriptors are based on two- or three-body correlations of atomic distribution. Recently, several limitations of these many-body descriptors in classifying different configurations were revealed, which have detrimental effects on the prediction of physical properties. We proposed a new class of descriptors based on persistent homology. We focused on the two-dimensional visualization of persistent homology, that is, a persistence diagram, as a descriptor of atomic configurations in the form of an image. We demonstrated that convolutional neural network models based on this descriptor provide sufficient accuracy in predicting the mean energies per atom of amorphous graphene and amorphous carbon. Our results provide an avenue for improving machine-learning potential using descriptors that depict both topological and geometric information.



Keywords

Topological data analysis, persistent homology, machine-learning potential, amorphous, convolutional neural network

Machine-learning potential is a promising candidate for resolving the trade-off between computational accuracy and cost for predicting the physical properties of complex systems. Various machine-learning models, such as Gaussian process regression^{1,2}, artificial neural networks^{3,4}, and their derivatives⁵⁻⁷, have been developed over the past decade. The details of the model structure are different for each technique. However, the basic strategy is the same: constructing a surrogate model of the relationship between atomic coordinates and physical properties, which can be used as an alternative to computationally demanding calculations.

Finding a suitable method to convert atomic coordinates into vectorial data is crucial for this purpose. To preserve the physically required symmetry of the target properties, the obtained vectorial representation of atomic coordinates, often called *descriptors*, should be equivalent to the translation, rotation, permutation of identical atoms, and reflection. Well-known examples of such descriptors are atom-centered symmetry functions (ACSF)^{3,8}, smooth overlap atomic positions (SOAP)^{9,10}, and many-body tensor representations¹¹. These previously proposed descriptors are generalized as many-body correlation functions of the atomic distributions¹². It has long been believed that descriptors based on three-body correlation provide an overcomplete description of atomic coordinates and are sufficient for predicting physical properties. However, several counterexamples of this belief have recently been revealed. As demonstrated by Pozdnyakov et al., descriptors constructed from two- and three-body correlation functions have fundamental limitations¹³. A different and efficient approach is required to construct descriptors that fulfill the symmetry restrictions.

In this letter, we propose a new descriptor constructed from persistent homology (PH). PH is an emerging technique in computational topology that is superior for extracting shape characteristics¹⁴⁻

¹⁶. This technique has been widely applied to the structural analysis of various types of condensed matter from biological molecules¹⁷ to glass¹⁸⁻²³. Recently, it has been demonstrated that PH is useful for determining the relationship between physical properties and atomic structures²⁴⁻²⁸.

In mathematics, a shape is considered as a topological space X consisting of a set of points (in our case, atoms) and topology. The topological characteristics of X are represented by the holes in space, which are encoded in an algebraic structure called the k -th homology group $H_k(X)$. A nested sequence of topological space $X_1 \subseteq X_2 \subseteq \dots \subseteq X_n$ provides the series $H_k(X_1), H_k(X_2) \dots H_k(X_n)$. The idea of PH involves tracking the elements of $H_k(X_i)$ as i increases. i represents the scale and is often referred to as “time.” The procedure used to obtain such a sequence is called *filtration*, which is schematically shown in Fig. 1. In the filtration process for 1-homology in a two-dimensional system, circles with radius r are placed at the respective atoms. Subsequently, r gradually increases. With increasing r , the circles start to intersect, and we set an edge between the centers of the circles. The growing network formed by these edges defines the sequence of the topological space X_i . A closed path formed by these edges corresponds to a topological feature, called a *cycle*. With a further increase in the radius, the closed path is fully covered by circles. This is interpreted as a cycle converting into another class of topological features called a *boundary*. The features of PH are represented by the pairs of birth and death times at which the cycles appear, and are converted into the boundaries. Filtration can be generalized into three or more dimensions using spheres or hyperspheres. The two-dimensional visualization of the pairs of birth and death times is called a persistence diagram (PD).

From the above definition, the PD of an atomic structure is invariant under the translation, rotation, permutation of identical atoms, and reflection. PD is expected to hold information on both connectivity and atomic distribution which is automatically collected during the construction of PH without manual

feature engineering. In addition, there is no restriction on the order of correlation during the construction of the PD, and the PD can include information on higher-order correlations. These points are supported by the PDs obtained from the cyclo-octane dataset used in Refs. 29,30. The dataset consists of the C atom positions in cyclo-octane molecules with 6,040 conformations. They were generated by introducing torsion angles with a fixed bond angle (115°) and bond length (1.52 \AA). Therefore, simple two- and three-body correlations between the nearest neighbors cannot distinguish configurations in this dataset. As shown in Figs. 2a and b, the PDs for the two configurations selected from the dataset show a visible difference.

Moreover, the difference from the conventional descriptors becomes evident upon comparing the results of the dimension reductions shown in Figs. 2c-f. The details of the analysis are summarized in the Supporting Information Section 1. The Cartesian coordinates of the eight C atoms in cyclo-octane are points in \mathbb{R}^{24} . The projection of $\mathbb{R}^{24} \rightarrow \mathbb{R}^3$ via principal component analysis (PCA) results in a surface that includes self-intersection (Fig. 2c). In Figs. 2d and e, similar embedded surfaces were obtained from the dimension reduction of high-dimensional vector representations based on the SOAP and ACSF descriptors. However, the PDs provided a different result from the others. The projection of PD descriptors on \mathbb{R}^3 forms a curve rather than a surface, as shown in Fig. 2f. Considering the strong constraint of the degrees of freedom in the ring-puckering coordinate of cyclo-octane³¹, the simpler structure obtained from the PD descriptor corresponds to a more efficient classification of configurations into typical conformers and their derivatives. For example, the edge point marked in red in Fig. 2f corresponds to 20 configurations in the dataset with a common twisted structure, as shown in the inset. Although the configurations were similar, they were placed at the separated points in other methods. This striking feature manifests the fundamental difference between the PD and the conventional methods in capturing the structural characteristics. Inspired by these results on a simple

system, we applied a PD as a superior descriptor of atomic coordinates for developing machine-learning potential to predict the mean energy per atom in complex amorphous structures.

Our targets in this study are amorphous graphene (aGr) and amorphous carbon (aC), which are two- and three-dimensional materials, respectively. To demonstrate that our methodology is not limited by specific computational conditions during data generation, we prepared the aGr and aC datasets using different methods. For aGr, the amorphous structures of 680 atoms were prepared via the melt-quench simulation of classical molecular dynamics (MD) using LAMMPS³². The dataset contains the atomic coordinates and total energies of 1,830 structures: 1,050 were sampled from the final state of the melt-quench simulations at different cooling rates, and 780 were sampled from the intermediate state in the simulations. For aC, samples were prepared via ab-initio MD melt-quench simulations using VASP³³⁻³⁶. Cubic cells of different sizes containing 216-atom were simulated to produce amorphous models with densities between 2.0 and 3.4 g/cm³. We performed 48 different MD runs and sampled intermediate structures from the trajectories of these MD runs. This resulted in a dataset of atomic coordinates and total energies for 12,960 structures. The detailed conditions for these calculations are provided in the Supporting Information Sections 2 and 3. Examples of the obtained structures are shown in Figs. 3a and b.

The descriptors of PH for the amorphous structures were constructed from a two-dimensional histogram of the PD on a 128×128 mesh. We focused on the square region $[0.0, 4.0]_{\text{birth}} \times [0.0, 4.0]_{\text{death}}$ for aGr, and $[0.0, 8.0]_{\text{birth}} \times [0.0, 8.0]_{\text{death}}$ for aC. Note that the units of these birth and death times were Å². As the PD reflects the number and size of the ring structures, the histogram values depend on the system size. Therefore, we converted the histogram into a probability distribution and standardized it to make the descriptors independent of the model size. We used the max-min standardization for aGr

and z-score standardization for aC. All the PD calculations were performed using the HomCloud package^{37,38}. A periodic boundary condition was imposed when calculating the PDs in aC because of the small model size.

This procedure yields descriptors with a format similar to that of grayscale images with a pixel size of 128×128 (Figs. 3c and d). These PDs encode the structural characteristics as the distribution of birth- and death-time, that is, how they appear as images. Based on this consideration, we constructed a learning model based on a convolutional neural network architecture that exhibited excellent image recognition performance. A schematic of the model is shown in Fig. 3e. The details of the model are described in the Supporting Information Section 4.1.

The results of training and testing of the learning model on the datasets of aGr and aC are shown in Figs. 4a and b. For aGr (aC), the root mean square error (RMSE) for the average energy per atom was 7.9 meV/atom (27.7 meV/atom) for the training data and 8.3 meV/atom (33.3 meV/atom) for the test data. The difference in RMSE between the training and test data was small, and the learning curve gradually decreased for both the test and training data (Supporting Information Section 4.1), indicating that overfitting was suppressed. The RMSE of the energy prediction in aC is comparable to that obtained using the Gaussian approximation potential (GAP) and high-dimensional neural network potential (HDNNP) for carbon reported in previous studies^{39,40}. In aC, the samples with mean energy per atom above -8.0 eV correspond to the liquid phase that appeared in the melt-quench simulation. In the liquid phase, there are no specific topological features such as medium-range order; nevertheless, the accuracy of the energy prediction using topological descriptors is maintained. This could be because PDs retain not only pure topological information (how the atoms are connected) but also geometric information (the distance and angle between atoms, and their correlations). We also verify

the ability of the model to interpolate. As summarized in Supporting Information Section 4.2, the model is robust to missing data in the middle-energy region, which indicates high interpolation ability.

A prerequisite for machine-learning potential is to maintain the accuracy of prediction when applied to a larger system size than that of the training data. Therefore, we predicted the mean energies per atom in aGr (aC) of 2,720 (512) atoms. The data for the larger amorphous structure and energy were generated using the same method as in the original data set. The prediction results are shown in Figs. 4e and f. The RMSE for the 2,720-atom system of aGr was 3.1 meV/atom, and that for the 512-atom system of aC was 33.6 meV/atom. These results indicate that the obtained machine-learning models fulfill the requirements. Furthermore, we visualized the activation mapping obtained from the outputs and gradients of the final convolution layer⁴¹ to clarify the basis of the prediction (for details, see Supporting Information Section 4.3). As shown in Fig. 4e, the learning model predicted the energy in aC for a high-energy liquid-like system based on the distribution of the birth–death pairs around the diagonal line. On the other hand, the distribution of birth–death pairs away from the diagonal line was focused on the low-energy amorphous sample (Fig. 4f). This flexibility of the attention region results in accurate prediction.

In summary, we constructed a new type of descriptor for atomic structures using PH. We proposed that a PD can be recognized as an image that encodes the information of the structure. We demonstrated that a convolutional neural network model based on a PD descriptor provides sufficient accuracy for predicting the mean energy per atom of amorphous structures. The idea of using a PD as the image data of atomic structures is a different methodology from the conventional descriptors based on the correlation of atomic distribution, and is expected to improve the reliability of machine-learning models for local and global physical properties. An area of future work will be to verify the

completeness of this descriptor together with a detailed comparison with conventional descriptors. The second is an improvement in the application of MD in large-scale systems. A possible direction is to construct a localized version of the PD to predict the local atomic energy contribution, as in HDNNP and GAP. It is also worth investigating whether this PD descriptor can be used in a complementary manner with the ACSF and SOAP as inputs to the HDNNP and GAP. A concrete way to achieve this is to use the global average pooling value in the final convolutional layer. Exploring these directions should further improve machine-learning potential by using descriptors that depict both topological and geometric information.

Associated content

Supporting Information

Analyses of cyclo-octane dataset; Computational setup for generating amorphous graphene dataset; Computational setup for generating amorphous carbon dataset; Machine-learning model

Author information

Corresponding Author

Emi Minamitani, Institute for Molecular Science, Okazaki 444-8585, Japan

Email: eminamitani@ims.ac.jp

ORCID: 0000-0002-8003-6526

Author

Ippei Obayashi, Cyber-Physical Engineering Informatics Research Core (Cypher), Okayama

University, Okayama 700-8530, Japan

ORCID: 0000-0002-7207-7280

Notes

The authors declare no competing financial interests.

Acknowledgements

This study was supported by JST, PRESTO Grant Numbers JPMJPR1923, JPMJPR2198, and MEXT KAKENHI 21H01816, 19H02544, 19H00834, 20H05884, Japan.

Calculations were performed using a computer facility at the Research Center for Computational Science (Okazaki, Japan).

References

- ¹ A.P. Bartók, M.C. Payne, R. Kondor, and G. Csányi, *Phys. Rev. Lett.* **104**, 136403 (2010).
- ² W.J. Szlachta, A.P. Bartók, and G. Csányi, *Phys. Rev. B* **90**, 104108 (2014).
- ³ J. Behler and M. Parrinello, *Phys. Rev. Lett.* **98**, 146401 (2007).
- ⁴ J.S. Smith, O. Isayev, and A.E. Roitberg, *Chem. Sci.* **8**, 3192 (2017).
- ⁵ A.P. Thompson, L.P. Swiler, C.R. Trott, S.M. Foiles, and G.J. Tucker, *J. Comput. Phys.* **285**, 316 (2015).
- ⁶ V. Botu, R. Batra, J. Chapman, and R. Ramprasad, *J. Phys. Chem. C* **121**, 511 (2017).
- ⁷ A. V. Shapeev, *Multiscale Model. Simul.* **14**, 1153 (2016).
- ⁸ J. Behler, *J. Chem. Phys.* **134**, 074106 (2011).
- ⁹ S. De, A.P. Bartók, G. Csányi, and M. Ceriotti, *Phys. Chem. Chem. Phys.* **18**, 13754 (2016).
- ¹⁰ A.P. Bartók, R. Kondor, and G. Csányi, *Phys. Rev. B* **87**, 184115 (2013).
- ¹¹ H. Huo and M. Rupp, *ArXiv:1704.06439* (2017).
- ¹² M.J. Willatt, F. Musil, and M. Ceriotti, *J. Chem. Phys.* **150**, 154110 (2019).
- ¹³ S.N. Pozdnyakov, M.J. Willatt, A.P. Bartók, C. Ortner, G. Csányi, and M. Ceriotti, *Phys. Rev. Lett.* **125**, 166001 (2020).
- ¹⁴ A. Zomorodian and G. Carlsson, *Proceedings of the Annual Symposium on Computational Geometry* **274**, 347 (2004).
- ¹⁵ H. Edelsbrunner and J. Harer, *Computational Topology : An Introduction* (American Mathematical Society, 2010).
- ¹⁶ M. Buchet, Y. Hiraoka, and I. Obayashi, in *Nanoinformatics* (Springer Singapore, 2018), pp. 75–95.
- ¹⁷ K. Xia and G.-W. Wei, *Int. J. Numer. Methods Biomed. Eng.* **30**, 814 (2014).
- ¹⁸ Y. Hiraoka, T. Nakamura, A. Hirata, E.G. Escobar, K. Matsue, and Y. Nishiura, *Proc. Natl. Acad. Sci. USA* **113**, 7035 (2016).
- ¹⁹ T. Nakamura, Y. Hiraoka, A. Hirata, E.G. Escobar, and Y. Nishiura, *Nanotechnology* **26**, 304001 (2015).
- ²⁰ Y. Onodera, S. Kohara, P.S. Salmon, A. Hirata, N. Nishiyama, S. Kitani, A. Zeidler, M. Shiga, A. Masuno, H. Inoue, S. Tahara, A. Polidori, H.E. Fischer, T. Mori, S. Kojima, H. Kawaji, A.I. Kolesnikov, M.B. Stone, M.G. Tucker, M.T. McDonnell, A.C. Hannon, Y. Hiraoka, I. Obayashi, T. Nakamura, J. Akola, Y. Fujii, K. Ohara, T. Taniguchi, and O. Sakata, *NPG Asia Materials* **12**, 85 (2020).
- ²¹ M. Murakami, S. Kohara, N. Kitamura, J. Akola, H. Inoue, A. Hirata, Y. Hiraoka, Y. Onodera, I. Obayashi, J. Kalikka, N. Hirao, T. Musso, A.S. Foster, Y. Idemoto, O. Sakata, and Y. Ohishi, *Phys. Rev. B* **99**, 45153 (2019).
- ²² S. Hong and D. Kim, *J. Phys. Condens. Matter* **31**, 455403 (2019).
- ²³ S.S. Sørensen, C.A.N. Biscio, M. Bauchy, L. Fajstrup, and M.M. Smedskjaer, *Science Adv.* **6**,

eabc2320 (2020).

²⁴ Y. Jiang, D. Chen, X. Chen, T. Li, G.W. Wei, and F. Pan, *Npj Computational Materials* **7**, (2021).

²⁵ J. Townsend, C.P. Micucci, J.H. Hymel, V. Maroulas, and K.D. Vogiatzis, *Nat. Commun.* **11**, 1 (2020).

²⁶ G. Kusano, K. Fukumizu, and Y. Hiraoka, in *33rd International Conference on Machine Learning, ICML 2016* (2016), pp. 2948–2957.

²⁷ E. Minamitani, T. Shiga, M. Kashiwagi, and I. Obayashi, *J. Chem. Phys.*, in press (2022).

²⁸ X. Chen, D. Chen, M. Weng, Y. Jiang, G.W. Wei, and F. Pan, *J. Phys. Chem. Lett.* **11**, 4392 (2020).

²⁹ S. Martin, A. Thompson, E.A. Coutsiyas, and J.P. Watson, *J. Chem. Phys.* **132**, 234115 (2010).

³⁰ B.J. Stolz, J. Tanner, H.A. Harrington, and V. Nanda, *Proc. Natl. Acad. Sci. USA* **117**, 19664 (2020).

³¹ W. Zou, Y. Tao, and E. Kraka, *J. Chem. Phys.* **152**, 154107 (2020).

³² S. Plimpton, *J. Comput. Phys.* **117**, 1 (1995).

³³ G. Kresse and J. Hafner, *Phys. Rev. B* **49**, 14251 (1994).

³⁴ G. Kresse and J. Hafner, *Phys. Rev. B* **47**, 558 (1993).

³⁵ G. Kresse and J. Furthmüller, *Comput. Mater. Sci.* **6**, 15 (1996).

³⁶ G. Kresse and J. Furthmüller, *Phys. Rev. B* **54**, 11169 (1996).

³⁷ HomCloud, <https://homcloud.dev/index.en.html>.

³⁸ I. Obayashi, T. Nakamura, and Y. Hiraoka, *J. Phys. Soc. Jpn.* **91**, (2022).

³⁹ V.L. Deringer and G. Csányi, *Phys. Rev. B* **95**, 094203 (2017).

⁴⁰ J. Wang, H. Shen, R. Yang, K. Xie, C. Zhang, L. Chen, K.M. Ho, C.Z. Wang, and S. Wang, *Carbon* **186**, 1 (2022).

⁴¹ R.R. Selvaraju, M. Cogswell, A. Das, R. Vedantam, D. Parikh, and D. Batra, *Int. J. Comput. Vis.* **128**, 336 (2020).

⁴² L. Himanen, M.O.J. Jäger, E. v. Morooka, F. Federici Canova, Y.S. Ranawat, D.Z. Gao, P. Rinke, and A.S. Foster, *Comput. Phys. Commun.* **247**, 106949 (2020).

⁴³ H. Adams, T. Emerson, M. Kirby, R. Neville, C. Peterson, P. Shipman, S. Chepushtanova, E. Hanson, F. Motta, and L. Ziegelmeier, *J. Mach. Learn. Res.* **18**, 1 (2017).

⁴⁴ I. Obayashi, Y. Hiraoka, and M. Kimura, *Journal of Applied and Computational Topology* **1**, 421 (2018).

Figure captions

Figure 1

Schematics of the filtration procedure used to obtain a PD from the data points. In this example, there are five points (a, b, c, d, and e). The PH group obtained by filtration is represented by two birth–death pairs A and B in the PD. The values of (birth time and death time) were (0.96,1.02) at A and (1.05, 1.30) at B. Pair A (B) corresponds to the birth and death of the cycle defined by the closed path a-b-c-a (c-b-d-e-c). The grey-shaded polygon in the growing sequence of topological space indicates that the closed path formed by the edges of the polygon is fully covered by circles in the filtration.

Figure 2

a), b) PDs of two configurations in the cyclo-octane dataset. Insets are the structure models of the respective configurations. c)-f) Projections of high-dimensional data on \mathbb{R}^3 by dimensional reduction using PCA. In each figure, the x, y, and z axes represent the values of the 1st, 2nd, and 3rd principal components, respectively. c) Result obtained from the Cartesian coordinates of eight C atoms. d) and e) Results obtained from the SOAP and ACSF descriptors of eight C atoms. These descriptors were constructed using the DDescribe package⁴², and considered as points in \mathbb{R}^{2016} and \mathbb{R}^{352} , respectively. f) Projection of the descriptors in \mathbb{R}^{15278} constructed from PDs using a persistent image^{43,44}. The red points in c)-f) correspond to the 20 configurations assigned to the end point of the curve in f). The details of the parameters used in SOAP and ACSF and the persistent image descriptors are summarized in Supporting Information Section 1.

Figure 3

Examples of the amorphous structures of a) graphene (aGr) and b) carbon (aC). c) and d) Descriptors constructed from the PDs for the structure shown in a) and b). The difference in the distributions and values in the two descriptors is due to the different focus areas and standardization methods during the data processing from the original PDs to the descriptors. e) Machine-learning model used in this study. The model consists of three convolution layers (conv) and two fully connected layers (FC). A max pooling layer (Max Pool) for downsampling is placed after each convolution layer. The size of the filter is 3×3 in all the convolution layers.

The first two convolution layers had 64 channels, and the last one had 32 channels. This model structure results in the input size of the first fully connected layers is $(128/8) \times (128/8) \times 32 = 8192$.

Figure 4

Comparison between the calculation results and predictions by the machine-learning model on the mean energies per atom in a) aGr and b) aC. The red (blue) dots are comparisons on test (training)

data. The predictions of the mean energies per atom for larger systems using the same model for aGr and aC are summarized in b) and c). e) and f) Activation maps for high- and low-energy samples in the aC dataset. The parameters used in the machine learning are summarized in Supporting Information Section 4.1.

Figure 1

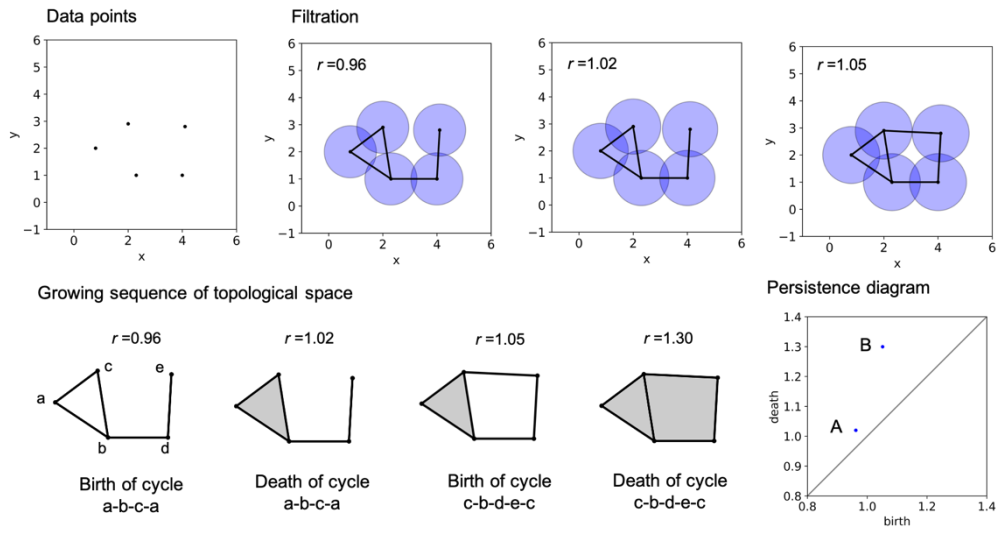
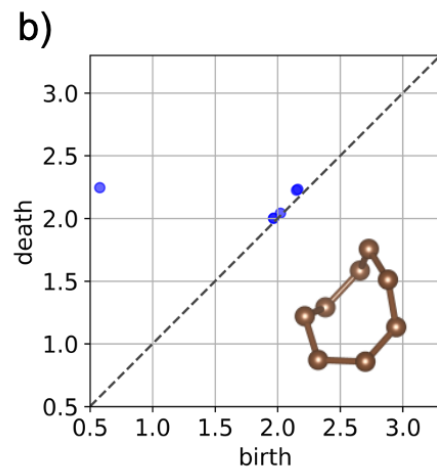
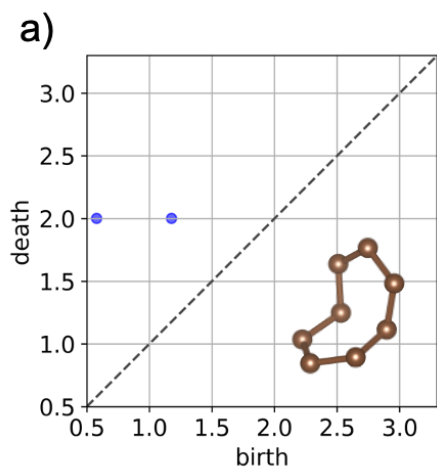
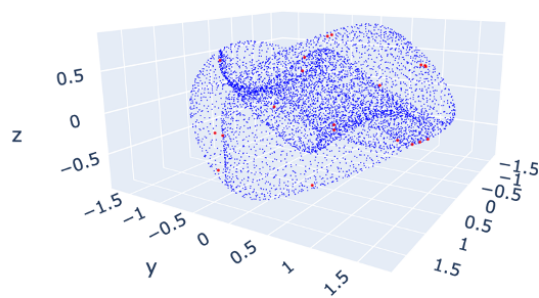


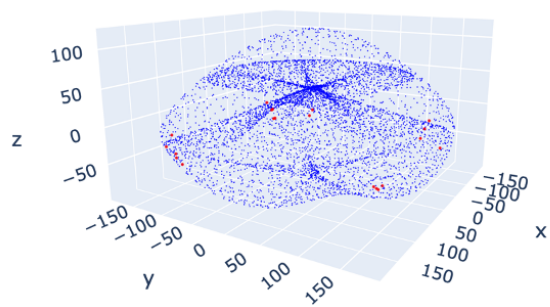
Figure 2



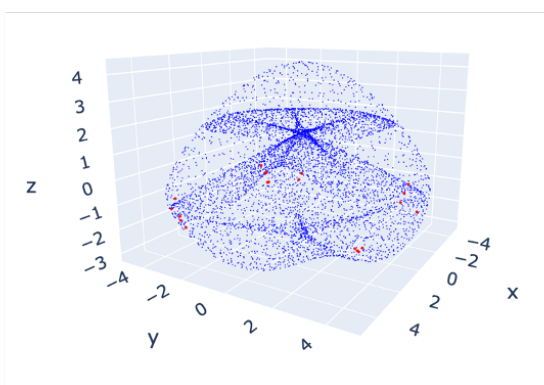
c) PCA



d) SOAP+PCA



e) ACSF+PCA



f) PH+PCA

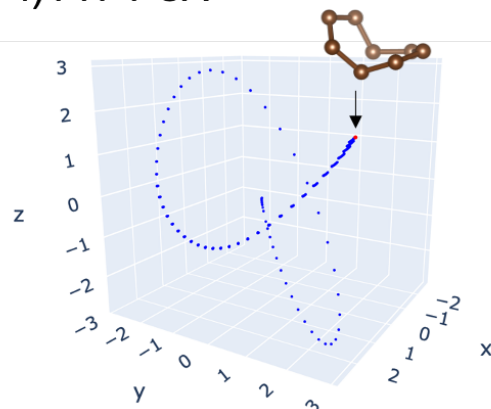


Figure 3

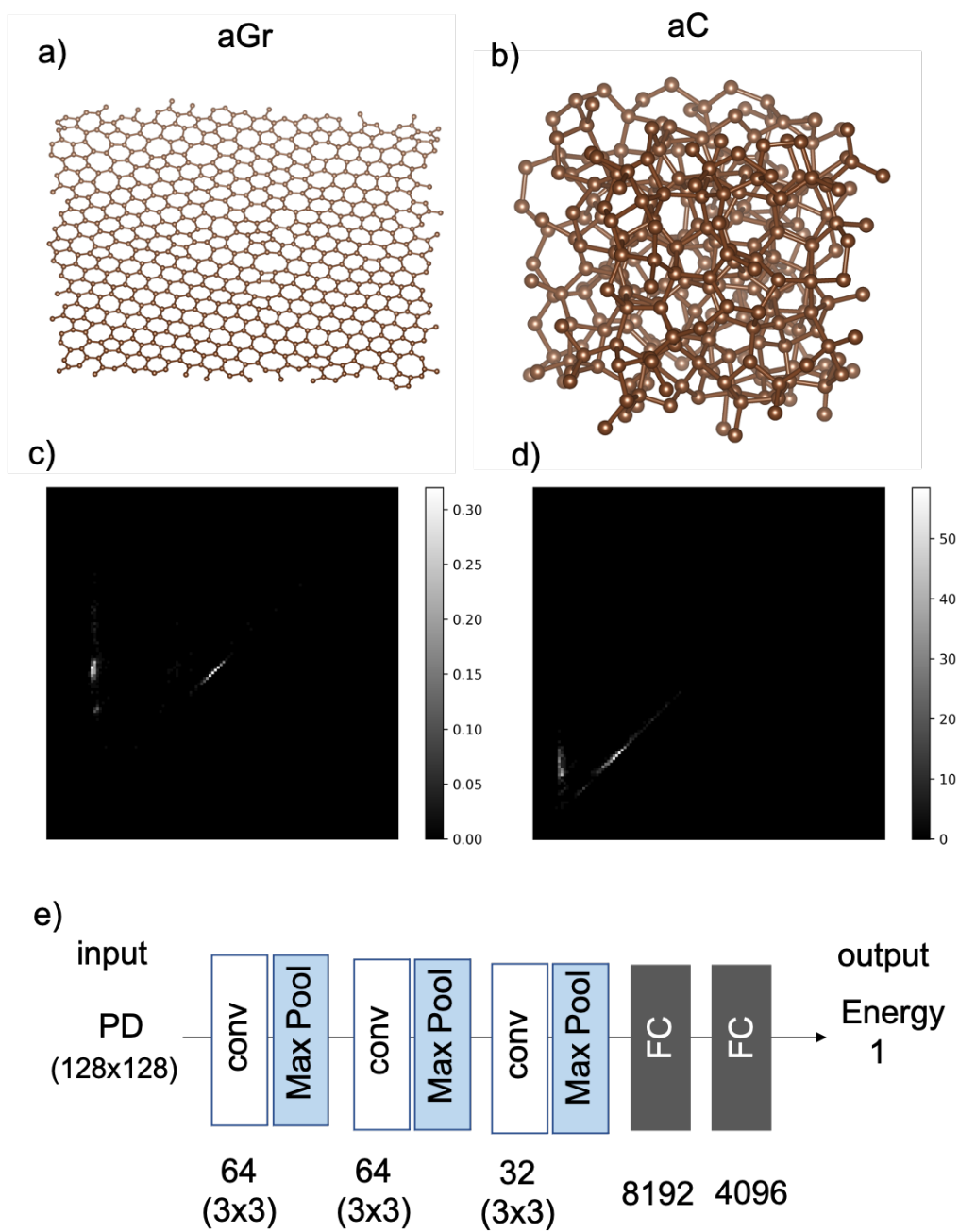


Figure 4

